Topology Aware Vector Field Denoising

Renata Nascimento, João Paixão, Hélio Lopes and Thomas Lewiner
Matmidia Laboratory – Departament of Mathematics – PUC-Rio – Rio de Janeiro – Brazil
http://www.matmidia.mat.puc-rio.br/{renata,jarpao,lopes,tomlew}

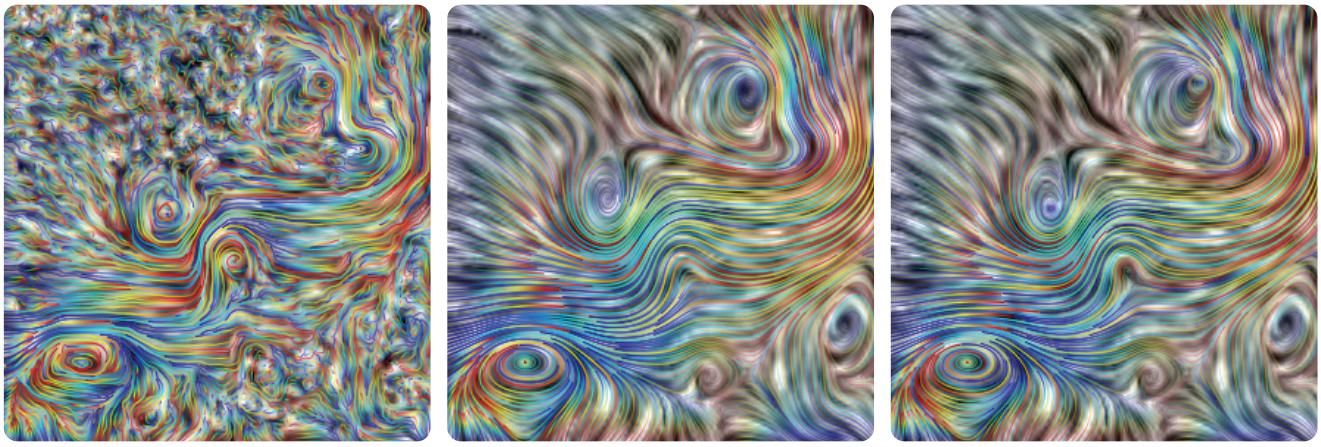

Figure 1. Topology-aware denoising of a measured fluid velocity field: (left) original field, (middle) gaussian denoising, (right) gaussian denoising preserving topological singularities selected through our interface.

***Abstract*—Recent developments in data acquisition technology enable to directly capture real vector fields, helping for a better understanding of physical phenomena. However measured data is corrupted by noise, puzzling the understanding of the phenomena. This turns the task of removing noise, i.e. denoising, an essential preprocessing step for a better analysis of the data. Nonetheless a careful use of denoising is required since usual algorithms not only remove the noise but can also eliminate information, in particular the vector field singularities, which are fundamental features in the analysis. This paper proposes a semi-automatic vector field denoising methodology, where the user visually controls the topological changes caused by classical vector field filtering in scale-spaces.**

***Keywords*- Vector Fields; Topology; Scale-Spaces; Denoising.**

I. Introduction

Denoising is the process of removing noise from a signal. It plays an important role as preliminary step for modeling and analysis. The main reason is that any measuring device are inherently susceptible to noise. As a consequence, signal processing should filter out uncertain information contained in the measured data in order to obtain a clean model. In real data, noise can have magnitude in average similar to the signal although not at coincident locations. Therefore, filtering out the noise without losing important information is, for sure, a very challenging task. In this context, this paper proposes a semi-automatic topology-aware denoising methodology for vector field data.

We focus here on vector fields and their topology since the interpretation of several physical behaviors, in particular fluid dynamics, is eased by a the detection and identification of its singularities, like sinks, sources and saddles. Moreover, several recent devices allow for measuring such vector fields: For example, *Particle Image Velocimetry* (PIV) [1] is an imaging technique to measure fluid velocity field that has been used on several applications in aerodynamics and hydrodynamics research. However, such real data is typically corrupted by noise, which harms singularity detection and further analysis, puzzling the interpretation.

Classical denoising approaches, such as convolution filters [2], [3], [4], [5], [6], rely on the assumption that the information is present in the measured data at a stronger scale than noise. Successive applications of such convolution filters noise generate a scale space [7], [8] representing the original data hierarchically, helping for subsequent analysis, in particular topological singularities [9], [10]. However, reconstructing such vector field using a single scale may keep either both noise and information or neither, leading to a delicate tradeoff. The main characteristic of the vector field denoising methodology to be presented is that the user controls the topological changes caused by classical vector field filtering by the use of a suitable interface. The main part of the user interaction is to provide local tradeoffs between information and noise. The reconstructed field is then a smooth combination of different denoising scales.

II. Related Work

Denoising: Among vector field filtering techniques on structured grids, several are specifically dedicated to colored image processing [11]. In particular, color image filters focus on the reduction of impulse noise [12], [13], [14]. More recently, Westenberg and Erlt [2] proposed a 2D vector field denoising algorithm that suppress additive noise by thresholding vector wavelet coefficients. Close to this work, a class of vector field filters has been introduced as generalized random walks: for images [15], meshes [16], [17] and vector fields [6]. This work will use random walk filters with Gaussian or anisotropic kernels as instances for the proposed methodology, since they naturally represent the original data in a hierarchical form as a scale space.

Scale spaces on vector fields: Scale-space techniques have become popular in computer vision for their capability to represent the multi-scale information inherently contained in real data. In particular, Bauer and Peikert [18] use scale spaces to track vortices in 2D-time dependent computational on fluid dynamics simulations. Klein and Ertl [9] proposes a strategy to track singularities over multiples scales in order to evaluate the importance of the critical points to the analysis and interpretation of the vector field. We propose here to employ such scale-space representations to let the user choose *locally* which scale to utilize for reconstruction.

Topology-aware techniques: Turbulent vector fields usually have structures in different scales that difficult their analysis. A possible solution to this problem is to analyze the topology of the vector field in order to automatically simplifying while keeping the most persistent features [19]. Another strategy, proposed in this work, relies on the user knowledge of the vector field, letting him decide interactively which topological singularities to keep or to smooth. Such approach has already been proposed in the field of surface reconstruction [20], [21].

III. Basic Concepts of Vector Fields

A *vector field* $\mathbf{v}$ on a planar domain $\mathcal{D} \subset \mathbb{R}^2$ is a function assigning to each point $(x, y) \in \mathcal{D}$ a 2D vector $\mathbf{v}(x, y) = (v^x(x, y), v^y(x, y))$. Assuming that v^x and v^y are differentiable bivariate functions, then the *Jacobian* matrix of $\mathbf{v}$ at point (x_0, y_0) is:

$$J_{\mathbf{v}}(x_0, y_0) = \begin{bmatrix} \frac{\partial v^x}{\partial x}(x_0, y_0) & \frac{\partial v^x}{\partial y}(x_0, y_0) \\ \frac{\partial v^y}{\partial x}(x_0, y_0) & \frac{\partial v^y}{\partial y}(x_0, y_0) \end{bmatrix}.$$

A point $(x_0, y_0) \in \mathcal{D}$ is *singular* for $\mathbf{v}$ if $\mathbf{v}(x_0, y_0) = (0, 0)$. Following Hartman-Grobman theorem, singular point can be partly classified by looking to the eigenvalues of the Jacobian matrix at that point:

- If the real parts of both eigenvalues are strictly negative, then the singular point is a *sink*.
- If the real parts of both eigenvalues are strictly positive, then the singular point is a *source*.
- If the eigenvalues are non-zero real number with different sign (one positive and one negative), then the the singular point is a *saddle*.
- If the real part of one of the eigenvalues is zero, the the singularity is of higher order.

In measured data, the vector field $\mathbf{v}$ is not given as a differentiable function. We will suppose here that we have the values of vector field $\mathbf{v}$ at the points (x_i, y_j) of a regular grid of size $M \times N$. We will denote $\mathbf{v}_{i,j} = (v^x_{i,j}, v^y_{i,j}) = \mathbf{v}(x_i, y_j)$, for $i = 1, \ldots, M$ and $j = 1, \ldots, N$. When needed, we can interpolate those values in-between the sample points. The simplest such interpolation is the bilinear interpolation:

$$\begin{aligned} \mathbf{b}_{i,j} &: [0, 1]^2 \to \mathbb{R}^2 \ , \\ \mathbf{b}_{i,j}(x, y) &= \mathbf{v}_{i,j} \cdot (1 - x)(1 - y) + \mathbf{v}_{i+1,j} \cdot x(1 - y) \\ &\quad + \mathbf{v}_{i,j+1} \cdot (1 - x)y + \mathbf{v}_{i+1,j+1} \cdot xy. \end{aligned} \quad (1)$$

IV. Topology-Aware Vector Field Filter

The basic idea of our methodology is to let the user locally select the noise scale to remove, defining a scale parameter $s(x, y)$ at each point. We start by generating a scale space from the original vector field and let the user choose a central scale s_0. In order to avoid the arduous task of defining the scale parameter $s(x, y)$ sample by sample, we display to the user the singularities that appear or disappear at different scales nearby s_0, where the distance can be set by the user as a scale difference or as a number of topological changes. When the user selects a topological change at a singular point (x_0, y_0), we define $s(x_0, y_0)$ to be the closest scale to s_0 that reverts the change. Finally, we return the reconstructed vector field as a smooth mixture of different scales of the scale space.

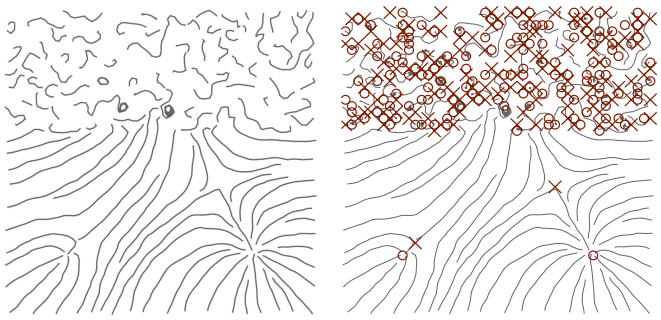

Figure 2. An artificial vector field represented by its streamlines (left) with its singularities marked (right).

Before entering in detail for each step, let's illustrate our technique on the example of Figure 2. This field contains some relatively clean parts at the bottom, and noisy parts at the top. The singular points at the bottom should be retained, almost all the singularities at the top should be cleaned, except for a sink that many streamlines point to.

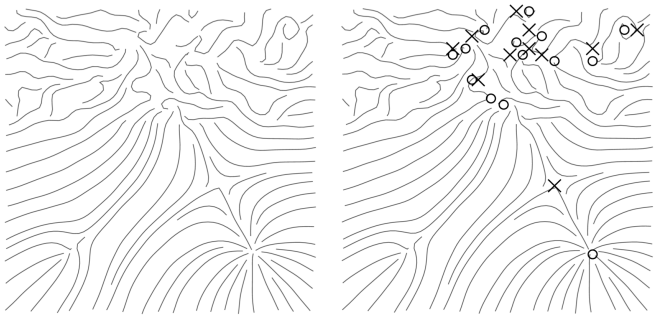

Figure 3. The vector fields at scale $s_0 = 10$ of its Gaussian scale space (left) with its singularities marked (right).

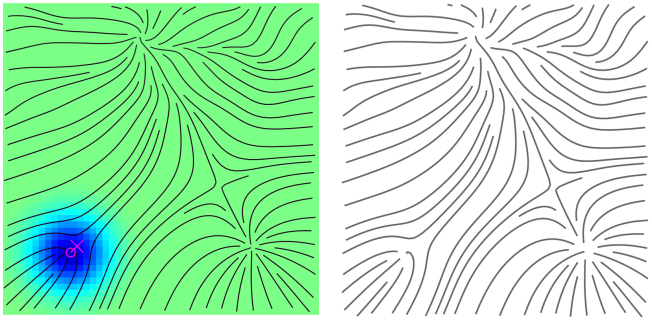

Figure 5. We finally interpolate the scales indicated by the user into a smooth function (left) which defines the reconstructed vector field (right).

Scale-space: In this example, we use a simple Gaussian filter to generate a scale-space (see Figure 3). Our method can build on any denoising scale-space, as exemplified in Section V using isotropic or anisotropic filters.

Singularity detection: All the vector fields of the scale space are available to the user at any time. Moreover, we display the singularities of the field in each scale. There are different methods to detect singularities however the detection mechanism can easily be replaced. In particular, we propose a new singularity detection, which tries to detect weak regions of the field, as detailed at Section VI. As it can been seen in Figure 3, even though the field is still noisy at scale $s_0 = 10$, the meaningful singularity shown in the bottom left of Figure 2 was lost in the denoising process. The top part of the field is still noisy, needing more denoising.

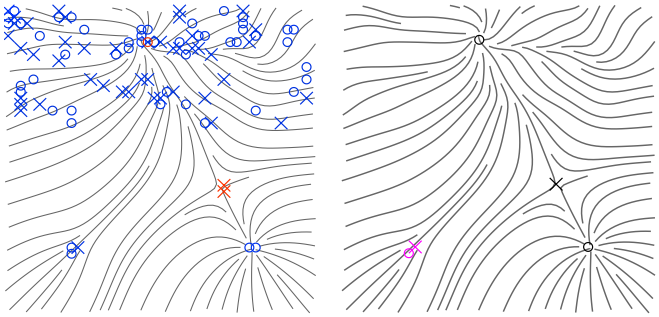

Figure 4. Our interface shows to the user the topological changes in nearby scales, here from 5 to 15 (left). The user then selects which topological changes he wants to revert (in purple on the right image).

Interface: In order to allow the user to denoise more of the top part while denoise less of the bottom to keep the meaningful singularity, we display to the user the topological changes at scales around 10 (see Figure 4). The user then selects which topological changes he wants to revert by a simple click.

Reconstruction: Each user selection defines a scale at the chosen point as the closest scale to $s_0 = 10$ that reverts the topological change. This gives a sparse sampling of the per-point scale parameter, which is smoothly interpolated to the whole domain. Our scheme supports different interpolations, and we provide two examples in Section VII. From this interpolation we can reconstruct an adaptively denoised vector field (see Figure 5).

V. Scale-space for Vector Field Filtering

The scale-space representation of the vector field is a collection of progressively denoised versions of the vector fields. Each version is associated to an increasing scale parameter s. We denote $\bar{\mathbf{v}}(s, x, y)$ the vector value of the field at scale s and point (x, y). The fundamental example of a scale-space on continuous vector fields is the Gaussian scale space, obtained by convolving with a Gaussian kernel of increasing variance: $G_\sigma(x, y) = \exp(-\frac{x^2+y^2}{2\sigma})$: $\bar{\mathbf{v}}(s, x, y) = \mathbf{v}(x, y) * G_s(x, y)$ [9].

In the discrete setting, this convolving approach fits into the more general framework of random walks [22], which ensures nice scale-space properties from local convolution masks. The scale parameter is then the number of convolutions applied. We exemplify our editing interface using two types of scale-space: using the Gaussian kernel G_σ and an anisotropic kernel [18], [6]:

$$A_{\sigma,\tau}(x, y, \mathbf{v}) = \exp\left(-\frac{x^2 + y^2}{2\sigma}\right) \exp\left(-\frac{||\mathbf{v}||^2}{2\tau}\right) ,$$

which takes into account the direction of the vector field and better preserves discontinuities. The scale space is then directly generated by the repeated application of a 3×3 mask with the above kernels.

VI. Detection of singularities

We use two classical approaches for the detection of critical points on a regular 2D grid. The first one is to search where the bilinear interpolation of the vector field vanishes. The second one computes the winding numbers of the same bilinear interpolation. Also we propose a detection of weak regions of the vector field, where the bilinear interpolation almost vanishes. This introduces a threshold, which let the user be more precise in his interaction.

A. Singularities of the bilinear interpolation

In the bilinear interpolation case, the detection boils down to solving the system of quadratic equations $\mathbf{b}_{0,0} = (0,0)$, where $\mathbf{b}_{i,j}$ is defined in Equation (1). This can be explicitly solved by computing the roots of the polynomial in y:

$$\begin{aligned} & (\quad -v_{01}^x\, v_{00}^y + v_{01}^x\, v_{10}^y + v_{11}^x\, v_{00}^y - v_{11}^x\, v_{10}^y + \\ & \quad +v_{00}^x\, v_{01}^y - v_{00}^x\, v_{11}^y - v_{10}^x\, v_{01}^y + v_{10}^x\, v_{11}^y \quad) \quad \cdot \quad y^2 \\ + & (\quad 2\, v_{01}^x\, v_{00}^y - 2\, v_{00}^x\, v_{01}^y - v_{11}^x\, v_{00}^y - \\ & \quad -v_{01}^x\, v_{10}^y + v_{10}^x\, v_{01}^y + v_{00}^x\, v_{11}^y \quad) \quad \cdot \quad y \\ + & \quad v_{00}^x\, v_{01}^y - v_{01}^x\, v_{00}^y \end{aligned}$$

To obtain the value of the x coordinate of the singular point we use the following expression:

$$x = \frac{(v_{00}^y - v_{01}^y)\cdot y - v_{00}^y}{(v_{00}^y - v_{10}^y - v_{01}^y + v_{11}^y)\cdot y - v_{00}^y + v_{10}^y} \ .$$

Eventually, this system may degenerate to a lower degree polynomial. It can then have zero, one or two solutions. Each of them must be tested to lie in the quadrilateral.

B. Winding numbers

The winding number counts the number of turns the vector fields achieves along a given closed curve Γ. It can be computed from the angular component of the vector field $\theta(\mathbf{v})$ by:

$$w_\Gamma(\mathbf{v}) = \frac{1}{2\pi} \oint_\Gamma d\theta(\mathbf{v})$$

This winding number is zero if the region inside Γ does not contain critical points. If Γ contains a single saddle, then $w_\Gamma(\mathbf{v}) = -1$. If it contains a single sink or source, it will be +1.

We compute the winding number for each cell of the discrete grid using for Γ the square that bounds the cell. With the linear interpolation on edges, we get the contribution of edge $(x_0, y_0) \to (x_1, y_0)$ to the above integral explicitly:

$$\begin{aligned} w_{00\to 10} = & \arctan\left(\frac{{v_{00}^x}^2 - v_{00}^x\, v_{10}^x - v_{00}^y\, v_{10}^y + {v_{00}^y}^2}{v_{10}^y\, v_{00}^x - v_{00}^y\, v_{10}^x}\right) \\ & - \arctan\left(\frac{v_{00}^x\, v_{10}^x - {v_{10}^x}^2 + v_{00}^y\, v_{10}^y - {v_{10}^y}^2}{v_{10}^y\, v_{00}^x - v_{00}^y\, v_{10}^x}\right) \end{aligned}$$

Summing over the four edges gives the desired winding number.

C. Weak regions

Finally we propose a method to detect weak regions. Instead of searching for zero values of the vector field, we give some leeway, controlled by the parameter ε, to find "almost singular" points. Formally, we search for

$$(i,j) \text{ such that } \min\|\mathbf{b}_{i,j}\| \leq \varepsilon.$$

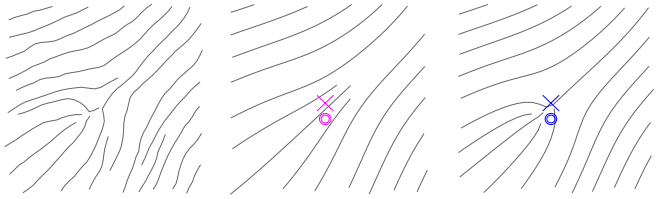

Figure 6. A weak region of a vector field, with no singular point ($\mathbf{b}(x,y) \neq 0$ and $w = 0$) (left). Using the weak region detection, we can let the user keep the vector field close to the original one near the "almost singular" point (middle). Selecting those points better preserves the original features of the vector field (right).

This reduces to find the roots of a 3^{rd} degree polynomial system in two variable, which leads to a 5^{th} degree polynomial in one variable.

This is useful in our context, since some regions of the vector field may contain too few singularities, but still requires adapted scale to preserve weak subregions (see Figure 6).

D. Singularity classification

For the reader interested in implementing a classification of the singularities, we provide the explicit Jacobian matrix of the bilinear interpolation $\mathbf{b}_{00}$:

$$\begin{bmatrix} v_{11}^x\, y - v_{00}^x\, \bar{y} + v_{10}^x\, \bar{y} - v_{01}^x\, y \ ; \ v_{11}^x\, x - v_{00}^x\, \bar{x} - v_{10}^x\, x + v_{01}^x\, \bar{x} \\ v_{11}^y\, y - v_{00}^y\, \bar{y} + v_{10}^y\, \bar{y} - v_{01}^y\, y \ ; \ v_{11}^y\, x - v_{00}^y\, \bar{x} - v_{10}^y\, x + v_{01}^y\, \bar{x} \end{bmatrix} ,$$

where $\bar{x} = 1 - x$ and $\bar{y} = 1 - y$. The eigenvalues are directly computed using the trace and determinant of the matrix.

The topological changes we can display to the user correspond to the creation, destruction, or change of type of a singularity at a fixed grid point.

VII. Reconstruction

The singularities selected by the user provides a sampling of the scale function $s(x,y)$ on the domain. To reconstruct the whole vector field, we need to interpolate this sampling. Denoting $\bar{\mathbf{v}}_{i,j}(s)$ the vector field sample at scale s, we define the reconstructed vector field $\tilde{\mathbf{v}}$ at grid point (x_i, y_j) by:

$$\tilde{\mathbf{v}}_{i,j} = \bar{\mathbf{v}}_{i,j}(s(x_i, y_j)) \ .$$

Virtually any interpolation scheme may work, although with different resulting qualities. If the interpolation is not smooth enough, the rapid changes in the scale parameter may create artifacts in the reconstructed field. Moreover, the interpolation must maintain the scale in a neighborhood of the singularity to preserve it. We implemented two methods for the interpolation of s that gave satisfactory results: radial basis functions (RBF), with Gaussian basis, and kernel Shepard interpolation [23] with Gaussian kernel.

The RBF interpolation of $s(x, y)$ from the scales of the used selected singularities s_k at (x_k, y_k) is obtained by a least-squares minimization on the coefficients α_k of

$$\min_{\{\alpha_k\}} \sum_k \|s_{rbf}(x_k, y_k) - s_k\|^2 \ , \quad where \tag{2}$$

$$s_{rbf}(x, y) = \sum_k \alpha_k G_\sigma \left(x - x_k, y - y_k\right) \ . \tag{3}$$

The kernel Shepard method modifies the original Shepard interpolation [24] by using kernels instead of the Euclidean distance:

$$s_{ks}(x, y) = \frac{1}{\sum_k G_\sigma(x - x_k, y - y_k)} \cdot \sum_k G_\sigma(x - x_k, y - y_k) \cdot s_k \ .$$

A important property of this method is that the image is limited to $[\min_k s_k, \max_k s_k]$.

VIII. Results

In this section we will present our experimental results on synthetic, simulated and measured vector fields. Since we work with relatively small 2D vector fields stored in regular lattices compared to the computing power of actual hardware, the interface responds in real-time to user interactions, except for the initial scale-space generation (see Table I). In all the experiments presented in this paper, the singularities detected by the winding number method and the bilinear one were the same, although they may differ in very particular cases. Moreover, those detected singularities are always a subset of the weak region detection, therefore only the interface and not the final results are not altered by the choice of the singularity detection method.

Synthetic data: We first validate our approach on a synthetic vector field, corrupted by an artificial, non-Gaussian noise (see Figure 7). We can denoise adaptively the vector field, recovering the original singularities. We use Gaussian scale-space with a kernel Shepard interpolation. Observe that, varying the σ of the kernel, we can carry larger portion of the fields at the selected scale.

Simulation data: We then experimented on a vector field of 2500 samples issued by a granular simulation [25]. The shearing of the granular system generates five main vortices between the shear bands, which are clearly visible in Figure 8 besides the noise. We use an anisotropic filter to generate the scale space, requiring around $s = 40$ steps to denoise the granular bands at the top and bottom. However, this smoothens out one of the main vortices. Selecting it in our interface allows to reconstruct a clean vector field with the main singularities, using here the RBF interpolation.

Measured data: We finally experimented our method on real measured vector field of 15624 samples, acquired through PIV imaging. The experiments of Figure 1 and Figure 9 are measured from a wall-jet setup, where water is injected from the left of the image and kicks on the wall

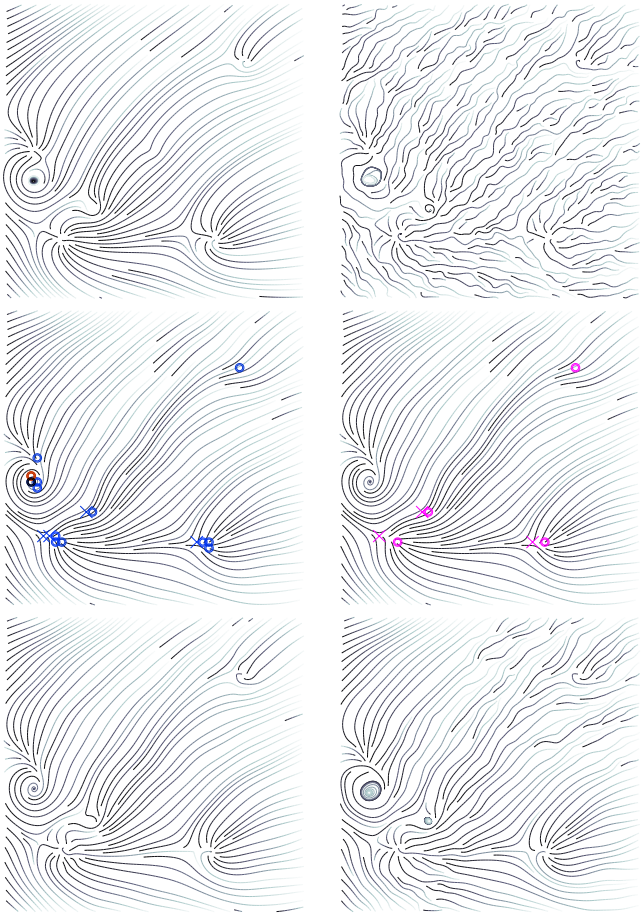

Figure 7. Experiments on an analytic vector field (top left) artificially corrupted by non-Gaussian noise (top right). The user can choose between singularities that disappeared before scale s_0 (in blue) or singularities that could be smoothed out at scale $s > s_0$ (in red) (middle left). From the user selection (middle right), we reconstruct the vector field maintaining the selected scale in a small (bottom left) or larger radius (bottom right).

on the right. The images correspond to the top half of the jet. The water injection is stronger in the experiment of Figure 1 as compared to the one of Figure 9. In both case, the top left part of the image is very noisy since there is less water, while the right part is turbulent. This leads to several important singularities on the right part of the field, which disappear before the singularities caused by the noise. In the reconstructed vector field, those singularities are recovered. We used a Gaussian scale-space for this experiment.

Table I
Timings, in milliseconds, for each step of the edition.

Data	**Fig**	**Size**	**Filter**		**Singularity**		**Scale**	**Reconstruction**		
			type	*(ms)*	*type*	*(ms)*	**select**	*type*	*solve*	*eval*
Analytic	7	2500	G_σ	18.9	w_Γ	98.0	7.3	KS		0.1
Granular	8	2500	$A_{\sigma,\tau}$	587.5	w_Γ	110.8	8.3	RBF	0.8	0.9
PIV 1	1	15624	G_σ	135.0	$\mathbf{b}=0$	947.6	65.6	RBF	0.1	7.6
PIV 9	9	15624	G_σ	182.8	$\mathbf{b} \leq \epsilon$	96.6	66.7	RBF	0.1	3.6

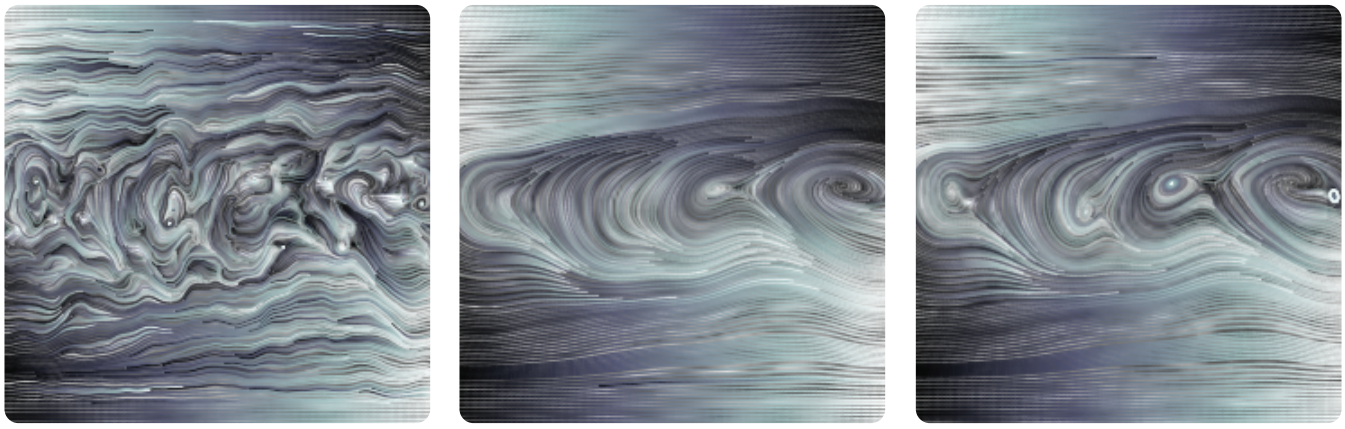

Figure 8. On a vector field from a simulated shear band granular system (left) 40 steps of denoising recovers the granular bands but loses one of the main vortices (middle). Selecting that vortex in our interface allow for a denoised reconstruction with the main singularities (right).

Limitations: The method proposed here has a few shortcomings. First of all the detection of singularities is only done locally and the reconstruction is done on a local base. Therefore, it does not handle non-local singularities such as a closed orbit. Also the technique works on a structured grid, while many recent vector field datasets are meshless to better take into account errors in the measure-point localization. Finally, large-scale denoising may displace the location of the singularity. Our interface then displays two very close-by topological changes, which are not relevant. A tracking of the singularities [26], [9] would certainly improve our technique on larger datasets.

IX. Conclusion

We proposed a methodology to denoise vector fields that takes advantage of the user knowledge of the data. Our interface displays topological contents to guide the user in adapting the local filtering scale in order to preserve important information while aggressively removing noise. The method supports different techniques for singularity detection, scale function interpolation or scale-space generation. Using 3D versions of each technique would allow to extend this work to 3D vector fields.

Acknowledgment

The authors would like to thank L.F. Alzuguir and J. Abrantes for the PIV data, and A. Bordignon for the granular simulation data. The authors would like to thank FAPERJ and CNPq for financial support during the preparation of this work.

References

[1] M. Raffel, C. Willert, and J. Kompenhans, *Particle Image Velocimetry: A Practical Guide*. Springer, 2002.

[2] M. A. Westenberg and T. Ertl, "Denoising 2D vector fields by vector wavelet thresholding," *Journal of WSCG*, vol. 13, no. 1-3, pp. 33–40, 2005.

[3] M. Lage, F. Petronetto, A. Paiva, H. Lopes, T. Lewiner, and G. Tavares, "Vector field reconstruction from sparse samples with applications," in *Sibgrapi*, 2006, pp. 297–304.

[4] M. Lage, R. Castro, F. Petronetto, A. Bordignon, G. Tavares, T. Lewiner, and H. Lopes, "Support vectors learning for vector field reconstruction," in *Sibgrapi*, 2009.

[5] M. Lage, A. Bordignon, F. Petronetto, Á. Veiga, G. Tavares, T. Lewiner, and H. Lopes, "Approximations by smooth transitions in binary space partitions," in *Sibgrapi*, 2008, pp. 230–236.

[6] J. Paixão, M. Lage, F. Petronetto, A. Bordignon, S. Pesco, G. Tavares, T. Lewiner, and H. Lopes, "Random walks for vector field denoising," in *Sibgrapi*, 2009.

[7] T. Lewiner, C. Ferreira, M. Craizer, and R. Teixeira, "Curvature motion for union of balls," in *Sibgrapi*, 2005, pp. 47–54.

[8] A. Bordignon, B. Vath, T. Vieira, C. Ferreira, M. Craizer, and T. Lewiner, "Scale-space for union of 3d balls," in *Sibgrapi*, 2009, pp. 9–16.

[9] T. Klein and T. Ertl, "Scale-Space tracking of critical points in 3D vector fields," in *TopoInVis*, 2005.

[10] F. Petronetto, A. Paiva, M. Lage, G. Tavares, H. Lopes, and T. Lewiner, "Meshless helmholtz-hodge decomposition," *Transactions on Visualization and Computer Graphics*, 2009.

[11] K. N. Plataniotis and A. N. Venetsanopoulos, *Color image processing and applications*. Springer, 2000.

[12] C. Tomasi and R. Manduchi, "Bilateral filtering for gray and color images," in *ICCV*, 1998, pp. 839–846.

[13] B. Smolka, R. Lukac, A. Chydzinski, K. N. Plataniotis, and W. Wojciechowski, "Fast adaptive similarity based impulsive noise reduction filter," *Real-Time Imaging*, vol. 9, no. 4, pp. 261–276, 2003.

[14] R. Lukac, K. N. Plataniotis, B. Smolka, and A. N. Venetsanopoulos, "Generalized selection weighted vector filters," *Journal of Applied Signal Processing*, pp. 1870–1885, 2004.

[15] M. Szczepanski, B. Smolka, K. N. Plataniotis, and A. N. Venetsanopoulos, "On the geodesic paths approach to color image filtering," *Signal Processing*, vol. 83, no. 6, pp. 1309–1342, 2003.

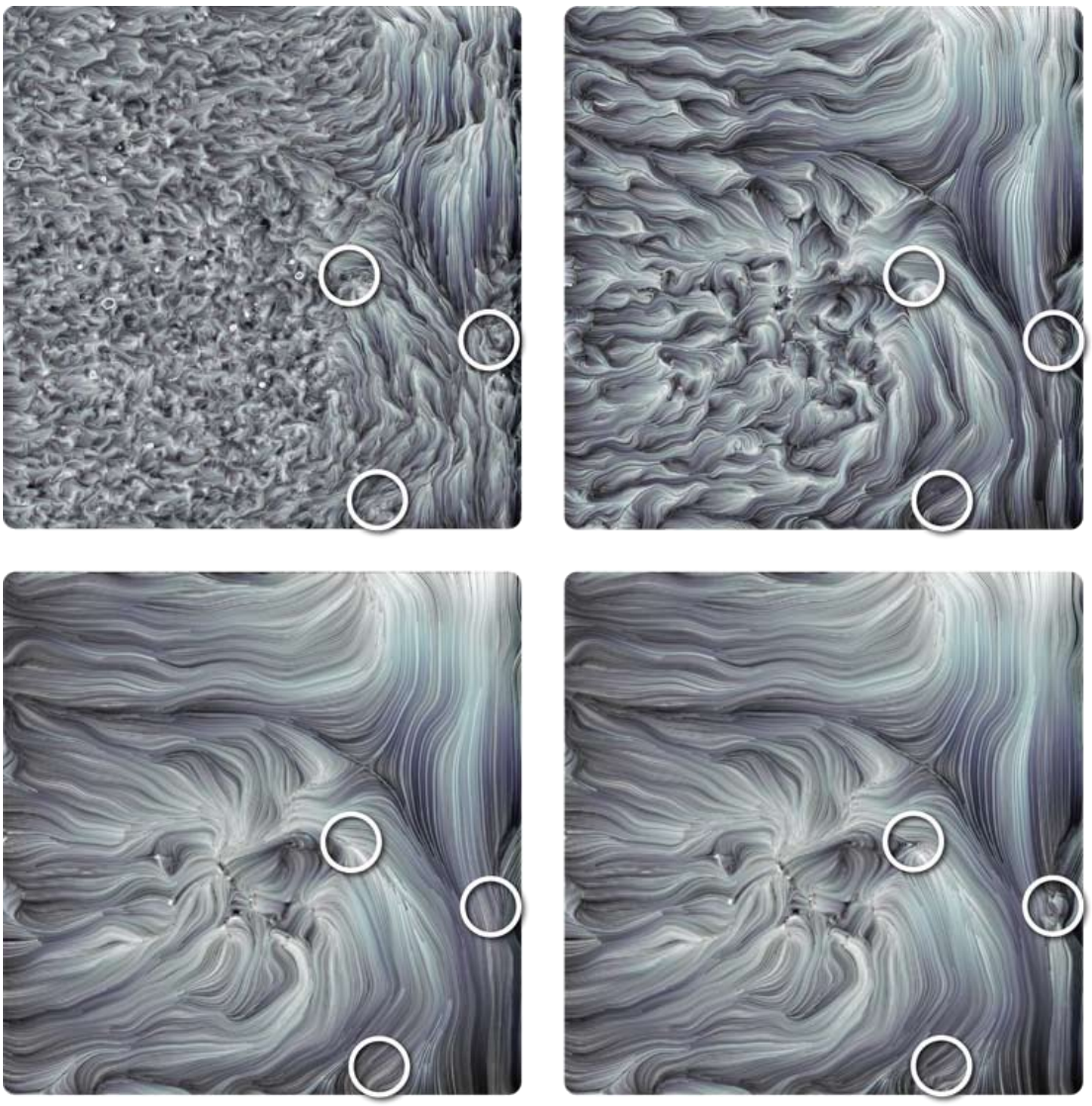

Figure 9. Denoising a vector field (top left) measured by a PIV device on a wall-jet experiment: the scale space at steps 30 and 100 (middle images) smoothens out the important singularities, at the right part of the image, while keeping some singularities related to the noise at the left part of the image. Selecting singularities at the right of the image better recovers the behavior of the fluid (bottom right).

[16] X. Sun, P. L. Rosin, R. R. Martin, and F. C. Langbein, "Random walks for mesh denoising," in *Solid and Physical Modeling*. ACM, 2007, pp. 11–22.

[17] ——, "Random walks for feature-preserving mesh denoising," *CAGD*, vol. 25, no. 7, pp. 437–456, 2008.

[18] D. Bauer and R. Peikert, "Vortex tracking in scale-space," 2002.

[19] X. Tricoche, "Vector and tensor field topology simplification, tracking, and visualization," Ph.D. dissertation, University of Kaiserslautern, 2002.

[20] T. Ju, Q.-Y. Zhou, and S.-M. Hu, "Editing the topology of 3d models by sketching," *Siggraph*, vol. 26, no. 3, p. 42, 2007.

[21] A. Sharf, T. Lewiner, G. Shklarski, S. Toledo, and D. Cohen-Or, "Interactive topology-aware surface reconstruction," *Siggraph*, vol. 26, no. 3, pp. 43.1–43.9, 2007.

[22] B. Smolka and K. W. Wojciechowski, "Random walk approach to image enhancement," *Signal Processing*, vol. 81, no. 3, pp. 465–482, 2001.

[23] J. Becker, "Método de interpolação de shepard baseado em núcleo," Master's thesis, PUC-Rio, 2002.

[24] D. Shepard, "A two-dimensional interpolation function for irregularly-spaced data," in *ACM national conference*, 1968, pp. 517–524.

[25] A. Bordignon, L. Sigaud, G. Tavares, H. Lopes, T. Lewiner, and W. Morgado, "Arch generated shear bands in granular systems," *Physica A*, vol. 388, no. 11, pp. 2099 – 2108, 2009.

[26] X. Tricoche, T. Wischgoll, G. Scheuermann, and H. Hagen, "Topology tracking for the visualization of time-dependent two-dimensional flows," *Computers & Graphics*, vol. 26, no. 2, pp. 249–257, 2002.